Progress In Electromagnetics Research, Vol. 147, 153–170, 2014

Design of Absorptive Coatings for Arbitrarily Shaped Targets for Reduction of Radar Cross Section (RCS) Using an Alternative to the Transformation Optics (TO) Algorithm

Raj Mittra* **and Yuda Zhou**

(*Invited Paper*)

Abstract—In this paper we present an alternative approach to addressing the problem of scattering reduction for radar targets, which have recently been dealt with by using the Transformation Optics (TO) algorithm which typically calls for the use of Metamaterials (MTMs) that are inherently narrowband, dispersive and highly sensitive to polarization as well as to the incident angle. The present design utilizes realistic lossy materials that can be conveniently fabricated in the laboratory, and are wideband as well as relatively insensitive to polarization and incident angle of the incoming wave. A modified interpretation of the TO algorithm is presented and is employed the design of RCS-reducing absorbers for arbitrarily shaped targets, and not just for canonical shapes, e.g., cylinders, for which cloaks have been designed by using the TO. The paper also briefly examines the topic of performance enhancement of absorbers by using graphene materials and embedded Frequency Structure Surfaces (FSSs). We begin by presenting the design procedure for planar absorbers, and then examine how well those designs perform for arbitrarily-shaped objects. Finally, we discuss how the planar design can be modified by tailoring the material parameters of the coating for specific object shapes. A number of test cases are included as examples to illustrate the application of the proposed design methodology, which is a modification of the classical TO paradigm.

1. INTRODUCTION

The objective of this paper is twofold. The first is to review the basic principles of the Transformation Optics (TO) approach, also known as Transformation Electromagnetics (TEM) algorithm, which has recently surfaced as one of the most innovative techniques for designing a wide variety of electromagnetic devices, including cloaks to render objects invisible. Our second goal is to present an alternative approach for designing absorptive coatings for scattering reduction, which differs from that used to design TO-based cloaks, and avoids the problems of narrow bandwidth and sensitivity to polarization and incident angle associated with the TO-based cloaks that we realize by using Metamaterials (MTMs).

The TO algorithm for designing cloaks is unique in that it provides a systematic approach, which is innovative as well as elegant, and is markedly different from the techniques that have been employed heretofore prior to the advent of the TO; for example, to design RCS-reducing absorbers.

The work has appeared earlier in e-journal FERMAT, which allows its authors to publish their paper elsewhere, after suitable modifications.

* Corresponding author: Raj Mittra (rajmittra@ieee.org).

The authors are with the EMC Lab, Department of Electrical Engineering, the Pennsylvania State University, State College, 16802 PA, USA.

2. FUNDAMENTALS OF TO

The principle upon which the TO is based has been enunciated in a number of papers, dating back to almost fifty years ago, that have examined the behavior of Maxwell's equations in a generalized curvilinear coordinate system. To explain the basic principle of the concept, let us consider two objects belonging to physical and virtual domains, and shown in Figures 1(a) and (b), respectively. The medium parameters surrounding these objects, namely (ε_1, μ_1) and (ε_2, μ_2), are also shown in Figure 1.

A number of prominent authors, among them Pendry [4], Leonhardt [10], Hao [12, 42, 43] Werner [11] and Kwon [44], as well as several others [13–26], have presented the relationship between the medium parameters in the two domains (physical and virtual) when we transform the geometry of object #2 in the virtual domain into that of object #1 in the physical domain via coordinate transformation, under the physical constraint that the electric and magnetic fields in the two domains remain "invariant" to the transformation between the two systems. The relationship can be explicitly stated as:

$$\Lambda = \begin{bmatrix} \dfrac{\partial x_1}{\partial x_2} & \dfrac{\partial x_1}{\partial y_2} & \dfrac{\partial x_1}{\partial z_2} \\ \dfrac{\partial y_1}{\partial x_2} & \dfrac{\partial y_1}{\partial y_2} & \dfrac{\partial y_1}{\partial z_2} \\ \dfrac{\partial z_1}{\partial x_2} & \dfrac{\partial z_1}{\partial y_2} & \dfrac{\partial z_1}{\partial z_2} \end{bmatrix} \tag{1a}$$

$$\begin{aligned} \bar{\bar{\epsilon}}_1 &= \frac{\Lambda \cdot \bar{\bar{\epsilon}}_2 \cdot \Lambda^T}{\det\,(\Lambda)} \\ \bar{\bar{\mu}}_1 &= \frac{\Lambda \cdot \bar{\bar{\mu}}_2 \cdot \Lambda^T}{\det(\Lambda)} \end{aligned} \tag{1b}$$

where Λ represents the Jacobian matrix relating the two domains (x, y and z can be any arbitrary curvilinear coordinate), and ε and μ represent the permittivity and the permeability of the corresponding mediums, respectively. Equation (1) enables us to navigate between the two systems and relate their material parameters in a unique, systematic and rigorous way.

Pendry [4], Smith [3] and a number of other workers [7–22] have leveraged the fact that the medium parameters can be related via Equation (1), in order to lay the foundations of the TO algorithm for designing cloaks, which render a target invisible when covered by using materials whose parameters are dictated by the TO. To explore the basic principles of the TO, we return to Figure 1 and define the following task for ourselves: design the cloak (i.e., a cover or a coating) for the PEC object in Figure 1(a) such that it is invisible to an arbitrary incident field that impinges upon it. Note that no restriction is being placed on the frequency, polarization or the angle of incidence of the illuminating field in connection with this task at this point.

To solve the problem posed above, we begin with a coordinate transformation, which morphs object #1, which is located in the physical domain, and for which we are trying to design the cloak, into object #2 residing in the virtual domain. Although this transformation is not obvious when the

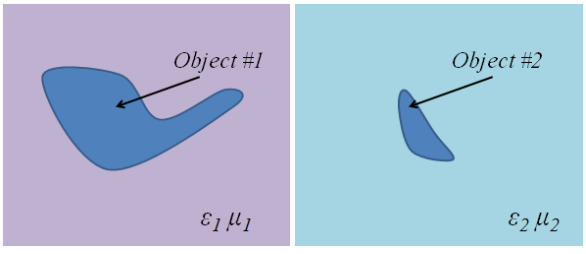

Figure 1. (a) Physical and (b) virtual domains used in the TO algorithm.

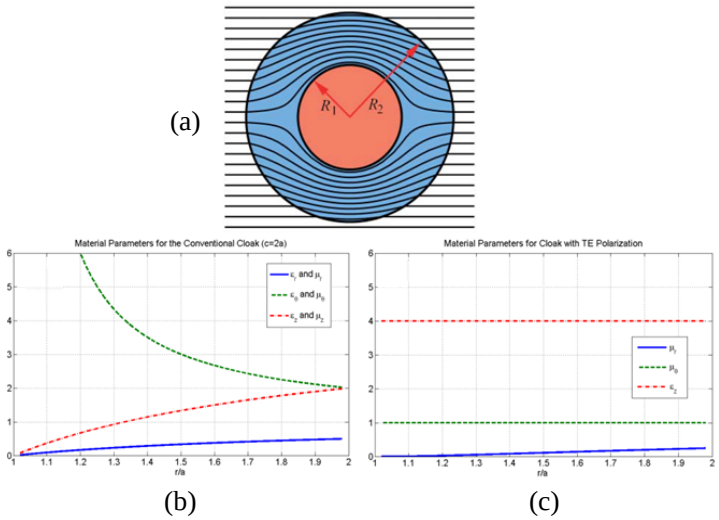

Figure 2. (a) Schematics for a cloaked PEC cylinder with $R_2 = 2R_1$, (b) material parameters for an all-angle, all-polarization cloak, (c) material parameters for a normal-incident, TE-polarization cloak from [9].

geometries of both the objects are totally arbitrary, it is nonetheless doable, at least theoretically. The caveat, is that the procedure provides us no guarantees that the materials parameters dictated by the transformation can be realized physically, and/or that they can be fabricated in practice to achieve cloak designs which satisfy the realistic specifications, such as small thickness, wide bandwidth, polarization insensitivity, etc..

The realizability issue, alluded to above, becomes even more critical when we attempt to design an "invisible" cloak, which is highly sought after by cloak designers. We will now explain why this is the case with a simple example as shown in Figure 2(a).

Let us assume, for the sake of convenience, that the target we wish to cloak is a cylinder. Following the TO paradigm, this problem has been extensively studied by a number of authors [1–22] and they have derived the material parameters for the cloak by invoking the TO, which makes the cloaked object disappear entirely (become invisible). In Figures 2(b) and (c) we plot the material parameters, presented in [9], that are required to make the cylinder invisible.

We observe several things from Figure 2. First, we see that the material parameters are anisotropic, and this in of itself can be problematic when we attempt to realize them in practice, because there is no systematic method available for synthesizing them. The second thing we observe about the required μ and ε values is that they vary over a wide range, tending to 0 in some regions and ∞ in others. Once again, this type of inhomogeneous behavior and a wide swing in the required material parameters as functions of the radial distance make it very difficult to realize them. In fact, we must resort to using Metamaterials (*aka* artificially-engineered materials) that are notoriously narrowband, dispersive and lossy when we attempt to realize the above type of material values. The above undesirable attributes that degrade the performance of the cloak and render it unsuitable for most applications requiring scattering reduction for real-world targets. What exacerbates the problem even more is the fact that the thickness of the cloak is comparable to the wavelength, rather than being a small fraction of the same. As we well know, a thin coating is desired in most applications; e.g., when designing stealth targets for the radar world.

At this point we return to the TO paradigm for cloak designs and scrutinize it carefully to see if we can thresh out the root causes of the difficulties that we have just identified with the TO-based design; namely anisotropy, high degree of inhomogeneity, dispersive nature, and large thickness. Although we have not mentioned this before, it is worthwhile to add dependence on the polarization and sensitivity to the incident-angle to the list above, which further aggravate the situation.

To identify the problem areas with the TO-based cloak designs, we turn to an alternate derivation

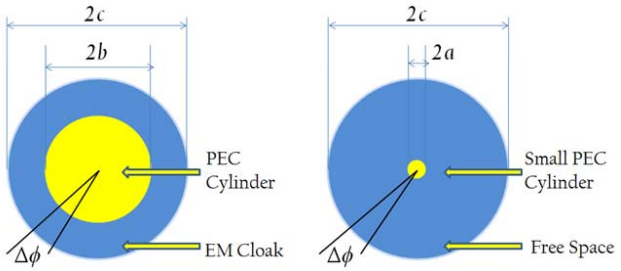

(a) (b)

Figure 3. TO-based cloak schematics and corresponding materials in the (a) physical geometry and (b) virtual geometry.

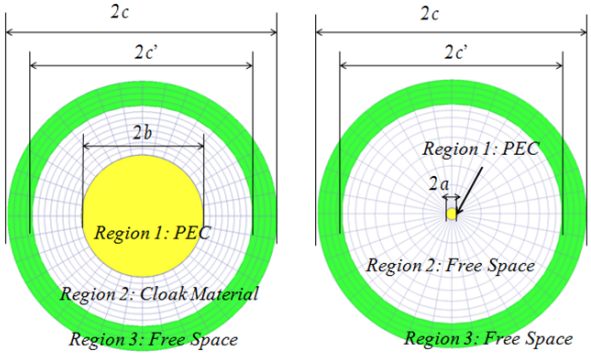

(a) (b)

Figure 4. Cloak problem with mesh schematics: (a) physical and (b) virtual domains.

of the material parameters in the context of Transformation Electromagnetics. Rather than relying directly on the Jacobian of the transformation, which relates the Physical domain to the corresponding virtual domain, we turn to the integral forms of Maxwell's equations appearing below:

$$\oint \mathbf{E} \cdot d\mathbf{l} = -\frac{\partial}{\partial t} \iint \mu \cdot \mathbf{H} \cdot d\mathbf{S} \tag{2a}$$

$$\oint \mathbf{H} \cdot d\mathbf{l} = \frac{\partial}{\partial t} \iint \epsilon \cdot \mathbf{E} \cdot d\mathbf{S} \tag{2b}$$

Initially, we consider the relatively simple case where the two domains are simply related by scaling, say by a factor 'γ', as has been done in the previous TO-based cloak designs [9]. The method we propose to relate the material parameters in the two domains is very general and is applicable to the case where the two geometries have arbitrary shapes, and are not simply related to each other by a scale factor, as we will discuss later in Section 3.

To derive the material properties of the physical domain, from the assumed parameters in the virtual domain (ε_0, μ_0 for free-space in this example), we turn to Figure 3 and Equation (2). The next step, we choose to impose the condition that the fields ($\mathbf{E_1}$, $\mathbf{H_1}$) in the physical domain be "identical" to those in the virtual domain, i.e., ($\mathbf{E_2}$, $\mathbf{H_2}$). To facilitate the imposition of this condition, we now discretize the two domains, as shown in Figure 4, by setting up a mesh to discretize the regions 2 and 3 in both domains. We take advantage of the circular symmetry of the geometries in the two domains, and of the fact that the geometry of the PEC cylinder, located in region-2 in the virtual domain is simply a scaled-down version of the one in the physical domain (region-1), and note that this transformation preserves the azimuthal symmetries of the two domains and, hence, the mesh size in the azimuthal direction remains unchanged when we navigate between the two domains. However, we follow a different strategy in the radial direction, along which we impose the following three conditions:

(i) The number of radial cells be identical in region-2 of the domains, which spans the radial distance $b < r < c'$ in the physical domain and $a < r < c'$ in the virtual domain (note we have chosen c', the outer radius of region-2 to be identical in both domains);

(ii) The cell size in the outermost boundaries of region-2 is to be identical in the two domains;

(iii) The cell sizes in region-3 in both domains be identically equal in the radial direction, not only between $c' < r < c$, but also beyond, i.e., $c < r < \infty$, meaning all the way to infinity.

There are logical reasons for imposing the above constraints, as we will now explain, before we proceed to derive the relationships between the material parameter distributions in the two domains. First, the TO must be applied to the entire region external to the PEC target — cylinder in this case

— when relating the material parameters in the two domains, viz., $b < r < \infty$ in the physical domain and $a < r < \infty$ in the virtual model. Specifically, we cannot truncate the regions as we transform from one domain to another, without introducing discontinuities in the fields, and thus violating the premise of TO under which we are operating. If we use condition (iii), in (2(a) and 2(b)), we immediately see that if the two fields as well as the mesh sizes would be identical in the two domains. It follows, then, that the material parameters must be exactly the same in regions-3 in the two domains. Since we have chosen the material parameters in the virtual domain in region-3 to be free-space, i.e., these parameters are ε_0 and μ_0, then region-3 in the physical domain must correspond to free-space as well, as would the parameters of the external region $c' < r < \infty$. This is a crucial point, and it implies that the cloak in the physical domain has but a finite thickness, spanning the region $b < r < c'$. This is obviously necessary in order for the cloak design to be practical, since we cannot accept a cloak design whose thickness is infinite, as it would be if we did not impose the equal-mesh-size condition in the two domains in region-3 and beyond; i.e., for $r > c'$. From (2), we can get:

$$E \cdot \Delta l = -\frac{1}{\Delta t}\mu \cdot H \cdot \Delta S \tag{3a}$$

$$H \cdot \Delta l = +\frac{1}{\Delta t}\epsilon \cdot E \cdot \Delta S \tag{3b}$$

where we are considering only the E_z and H_ϕ components for this 2D geometry, namely a cylinder, for which z is along the axis of the cylinder, and ε and μ in (3) are the appropriate elements of the $\bar{\bar{\varepsilon}}$ and $\bar{\bar{\mu}}$ tensors.

Let us now turn to the regions-2 in the two domains, namely physical and virtual. Recall that we have imposed the condition that the cell size at the outermost boundary of this region be identical in the two domains, which guarantees that the transition of the material parameters would be smooth as we transition from region-2 to region-3. (Recall region-3 and beyond is free-space in both domains). So, all that remains for us to do now is to determine the material parameters of the cloak region in the physical domain, which spans from $b < r < c'$, by invoking the condition that the fields ($\mathbf{E_1}$, $\mathbf{H_1}$) of the physical domain be identical to the fields ($\mathbf{E_2}$, $\mathbf{H_2}$) in the virtual domain (which we have chosen to be free space), as well as condition (i) on the number of cells in the two domains associated with region-2, namely that this number be identical in the two domains. At this point, we impose an additional condition, without loss of generality, that in the radial direction the cell sizes in region-2 in the physical domain be all equal, as we go from $r = b$ to $r = c'$. We also choose the cell size in the radial direction to be $\lambda/20$, though there is no hard and fast rule that says that we must adhere to this last condition, which is dictated more by the numerical discretization of the integral forms of Maxwell's Equation (3), than by anything else. At this point, we note that since the dimensions of region-2 in the physical and virtual domains are different, we typically choose the radius a such that $a \ll b$, in order to ensure that the scattering from the small cylinder in the virtual domain would be small — in fact vanishingly small in the ideal case — in order to render it invisible as $a \to 0$ in the limit. Note that we must choose a non-uniform mesh in the virtual domain, so that we can simultaneously satisfy condition (iii), as well as the constraint on the number of cells in the radial direction in the two domains; namely that they be equal. Though we have some flexibility in terms of the variation of the cell size in the radial direction in the virtual domain, we choose this variation in Δr to be smooth, and monotonically increasing in terms of the cell size as we go from $r = a$ to $r = c'$, so that the summation of all the $\Delta r'$s equal $(c' - a)$. An example of such a mesh is shown in Figure 5.

Having defined the meshes in the two domains, we finally turn to the task of determining the material parameters of the cloak in the physical domain. Recall that we wish to impose the criterion that the two sets of fields; namely ($\mathbf{E_1}$, $\mathbf{H_1}$) and ($\mathbf{E_2}$, $\mathbf{H_2}$) in the two domains, respectively, be identical. Equation (2) tells us that the (ε_1, μ_1) values in the physical domain, must be ε_0/γ_n and μ_0/γ_n, where γ_n is the ratio of the areas of the nth cell in the physical and virtual domains, respectively. It is evident that, under these conditions, the ε_1 and μ_1 must start out at ε_0/γ_1 and μ_0/γ_1, where γ_1 the ratio of the dimensions of the first cell (at $r = b$) in the physical domain to that of the dimension of its counterpart (at $r = a$) in the virtual domain. Also, we recall from our previous discussion, that ε and μ values are identical in both domains when we reach $r = c'$, and that they are both just (ε_0, μ_0), i.e., material parameters of free space.

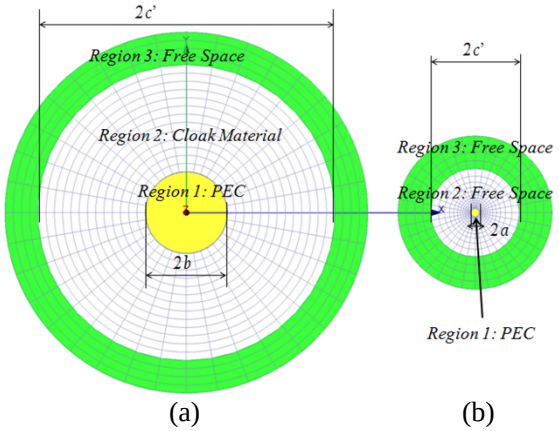

Figure 5. Cloak problem with mesh schematics: (a) physical and (b) virtual domains.

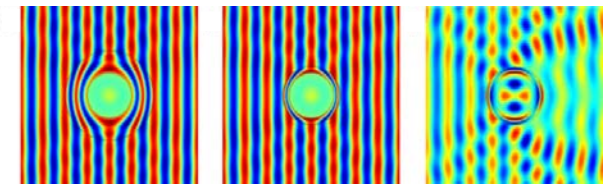

Figure 6. Field distribution for A PEC cylinder in (a) an ideal TO cloak, (b) an ideal, thin TO cloak, (c) a 3-layered TO cloak in which the medium parameters at each layer correspond to those of the ideal thin cloak.

We now make two important observations. First, the cloak we have designed by following the procedure just described, which is based on the TO algorithm — though implemented differently than via the use of the Jacobian — varies inhomogeneously in the radial direction, albeit smoothly. Second, the ε and μ values in the physical domain are larger, by a factor of $1/\gamma_1$, than their free-space counterparts. This factor is responsible for the root cause of difficulty encountered when designing TO-based cloaks, since it calls for Metamaterials to fulfill the requirements on the material parameters if we insist that the cloak must render the target totally "invisible". This is because we can fulfill that condition if and only if $a \to 0$, in the strictest sense, and this implies that γ_1 must also follow suit and tend to zero as well.

We should mention that although we chose the simple geometry of the cylinder to identify the fundamental difficulties with the implementation of the TO paradigm, the problem with the realization of material parameters persists regardless of the geometry of the target, as long as we insist that it becomes invisible, which in turn requires that the scale factor (equivalent to γ) tends to 0.

Before we discuss our strategy for overcoming this roadblock, we examine another fundamental limitation posed by the TO paradigm when we attempt to reduce the thickness of the cloak $t\,(= c' - b)$, to realistic values, e.g., a small fraction of the wavelength. We note that the material values $(\varepsilon_0,\ \mu_0)$ near the outer boundary of the cloak, located at $r = c'$, do not change, regardless of whether r is large or small, and for that matter, neither do the behaviors of $(\varepsilon,\ \mu)$ of the cloak in the neighborhood of $r = b$, where the above parameters $\to \infty$. While we can attempt to partially mitigate this problem by imposing a cap on the values of these parameters, we cannot change the fact that the relative ε_n and μ_n must reduce from very large values at the surface of the cylinder to unity within a relatively short distance. This, in turn, again poses realizability problems in practice. For this reason, practical realizability of thin invisibility cloaks have not met with too much success in the past, and it is unlikely that the thickness issue will be resolved anytime soon if we continue to impose the above invisibility criterion on the TO-based cloak designs. Figure 6 shows the deterioration of the performance of the cloak (see Figure 6(c) when we design a thin three-layer cloak by using discretized values of the cloak parameters, which vary continuously from $r = b$ to $r = c'$). It is evident that the wavefront of the field becomes considerably distorted when we compare the performance of the thin cloak with the ideal one the results for which are included in Figure 6(b) for comparison.

We now proceed to outline a strategy for designing coatings for radar targets which circumvent the various problems identified above, when attempting to realize realistic cloak designs.

3. RCS REDUCTION FOR PRACTICAL TARGETS BY USING A MODIFICATION OF THE TO CONCEPTS

We now present a modified version of the TO approach that attempts to overcome the major problems encountered in TO-based designs. We make it clear at the outset, our goal is to reduce the RCS, rather than attain invisibility.

Our strategy is to follow a three-step process, which we will now outline below. Our first step is to design wideband layered absorbers for infinite, planar, conducting ground planes. We note that this is also the basic approach to designing coating for radar targets to render them stealthy, regardless of their shapes and that it is relatively easy to carry out this design by using optimization algorithms to determine the material properties and the layer thicknesses to reduce the reflection from the coated PEC plane; say, below −10 dB level, and over a wide frequency band; say covering the radar frequencies from 2 to 18 GHz, for example. (Note that this is in contrast to 2–3% bandwidth of cloaks designed by using the legacy TO algorithm).

A typical cost function [40] to be minimized, which is suitable for optimizing the layer thicknesses while balancing the absorption performance and overall thickness can be defined as follows:

$$F = m * R_L + (1 - m) * \sum_{i=1}^{k} d_i \tag{4}$$

where d_i represents the thickness for each layer of the absorber; R_L stands for the reflection level at the air-absorber interface and is a function of the material parameters and thicknesses d_i of the absorbing layers (Figure 7); and m is the weight of the reflection level in the optimization, signifying the importance of the reflection level over the collective thickness of the layered absorber. Note that $m = 1$ corresponds to the case where the total thickness is predetermined, and only the reflection coefficient is minimized. Note that the parameters of the materials available to us are dispersive, and hence the optimization to determine the thicknesses should be carried out over the entire desired frequency band.

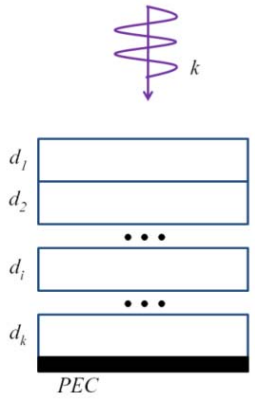

Figure 7. Model schematics of the optimization problem for the multilayer absorber.

Besides the wide bandwidth, one of two other important attributes which distinguish this type of coating design from the traditional TO cloaks is that the proposed blankets are relatively insensitive to polarization, mostly due to the fact that we have a wide range of homogeneous, isotropic materials available to be selected as absorbing layers. The incident angle of the impinging radar signal interrogating the target has a much wider tolerance range than that of the TO-based cloak. This is in contrast to the TO-designed cloaks [9], which become rapidly ineffective if either the polarization or the incident angle deviates even slightly from that of the combination of the two parameters for which the TO-cloak was designed.

The second attribute of the present design is perhaps even more crucial than the first one we mentioned above, and this concerns the availability of the materials needed to design the blanket,

which, as we might recall, posed serious realizability problems, owing to the unrealistically large (or small) parameter values (see Figure 2) demanded by the TO algorithm.

As is well known, the RAMs (radar absorbing materials) have been around for a very long time, some for many decades, dating back to when stealth aircrafts came into vogue in the sixties, and earliest theoretical and experimental work starting around 1930s. We realize that information on some of these RAM materials is not openly available because of their "classified" or "secret" nature, understandably so because they are used in military applications to design stealth aircrafts and missiles. Nonetheless, a plethora of information about similar absorbing materials is available in the open literature, including the details of their fabrication, which have been described in [27, 28], for instance.

Here we will use two different types of materials namely CoFe Nano-Flakes (NF) and CoFe Nano-Particles (NP), whose frequency variations are shown in Figure 8. We point out that these materials can be realized with relative ease, as is evident from [27, 28], where the details of their fabrication can be found.

We note that the ε and μ values of these materials are both complex and dispersive. We hasten to point out, however, that unlike the MTMs, which typically have variations with frequency because of resonant inclusions they use to achieve effective ε and μ values that are very high, very low, or even negative, the material parameters of the NP and NF materials vary relatively smoothly with frequency, and this is crucial for realizing wideband performance, as we shall soon see.

To illustrate the fact that we can indeed achieve wideband performance in terms of reflection reduction over a wide frequency band with relative small thicknesses of 2, 4, 6 and 7 layer absorbers we refer to Figure 9, in which a 10 dB (or better) reduction in the reflection coefficient is presented. Although not shown here, the results for the reflection coefficient reduction are also satisfactory when either the polarization, or the incident angle is varied and this is also true when both are changed simultaneously.

We now move to the second step in our design procedure, which is to adapt the blanket designed for the infinite PEC plane to an arbitrarily-shaped object. Initially we consider an object with a smooth surface whose radius of curvature is moderate-to-large everywhere. We will generalize the procedure in the third step, using the principles of the TO when the above assumption regarding the smoothness of the object is not valid, as for instance when the object has sharp edges or bumps, as a general target would in practice.

When the object has a relatively smooth geometry, we initially wrap the multilayer absorbing blanket, which we have designed earlier for the planar surface around the PEC target whose scattering cross-section we are attempting to reduce, and test the effectiveness of the blanket for the new object. For a wide variety of targets we have examined, a number of which are shown in Figure 10, we have found that the blanket does reduce the monostatic as well as the bistatic radar cross-section in the "reflection" region near the surface of the object for different angles of incidence and polarizations of

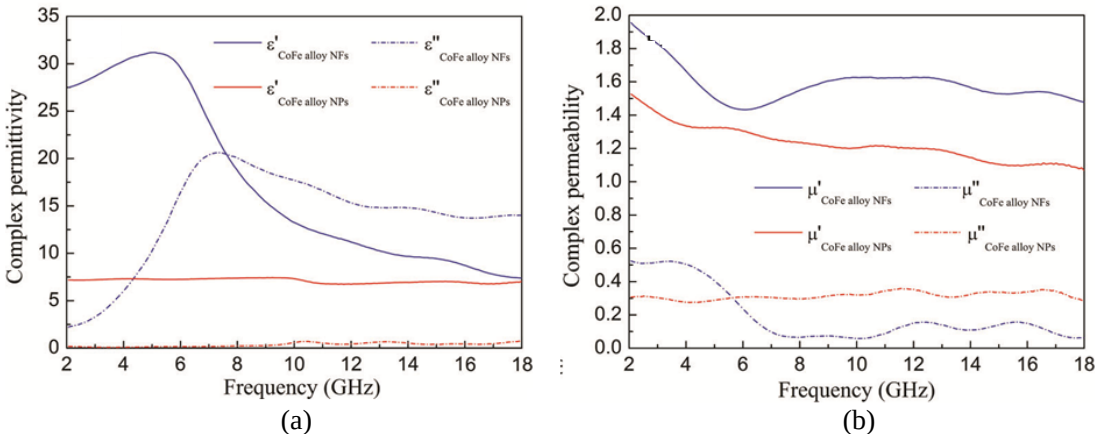

Figure 8. Real and imaginary parts of the (a) permittivity and (b) permeability for the two types of absorbing materials used in the multi-layer absorbing blanket design.

the incoming wave. The results for a two-layer absorber are shown in Figures 11 and 12 for a rectangular cylinder of finite length, which we have studied as a test case.

A simple test, which is typically applied to cloak designs, is to examine the wavefront of the total (incident + scattered) field, and see how the level of distortion of the wavefront decreases when the scatterer is covered by the layered absorbing coating. We present the plots of these wavefronts of the total fields for normal and oblique incidence cases for both polarizations in Figures 11 and 12, respectively.

We observe that the object, which is a finite cylinder of height 18 cm, generates distorted wavefronts owing to the contribution of the scattered field from the object, even when covered by a two-layer blanket, designed for the infinite planar PEC object, for the nominal frequency range of 4.6–18 GHz, with a nominal reflection coefficient of −10 dB or less. However, we also note from Figure 11 that the distortion in the phase front is relatively small once we go above the low end of the design frequency range, viz., 4.6 GHz for the planar geometry, confirming that the planar design performs reasonably well even though we are dealing with a rectangular cylinder now. We hasten to point out that the results presented in Figure 11 are not for a coating which has been optimized for the object at hand, and we expect some compromise in the performance of the coating. However, we can improve this performance by optimizing the parameters of the two-layer design, specifically the relative thicknesses of the two layers, even as we maintain the total thickness intact. We expect the changes to be relatively minor, however, except for the corner regions and, hence, the optimization process should be realistic as well as numerically feasible. The above remarks are also applicable to the oblique incidence case, for which some sample results are presented in Figure 12.

It is important to point out that the strategy for designing the absorptive coating, presented herein, is very different from that employed for ideal traditional TO cloak, since the latter is designed to render the (object + cloak) composite to have a *zero* scattering cross-section in *all* directions, whereas the blanket design introduced here seeks to reduce both backscattering and bi-static scattering scenarios but only in the *reflection* region, and not in the forward-scattering direction. We hasten to point out, however, that this type of performance is perfectly well suited for modern radar systems, symbolically depicted in Figure 13, where only the scattering in the reflection region is of concern [36–38].

For the final step, we consider the problem of absorber design when a shape perturbation is introduced in an object. Let us say that our modified target is the same rectangular cylinder we just considered above, except for a bump on the top surface. The extra corners introduced by the perturbation, be they smooth or sharp, would obviously introduce additional distortions in the planar phase front, and potentially increase the scattering level. Our objective here is to restore the field behavior so that it is close to that of the original object that we had prior to the introduction of the perturbation.

We now outline the procedure for the blanket design for the new object, shown on the left in Figure 14; i.e., Figures 14(a), (c), (e), which is in the physical domain, and is a modified version of the one shown in the right side of the same figure; i.e., Figure 14(b), (d), (f), which corresponds to the virtual domain. Note that unlike the cylinder example we discussed earlier, the medium in the virtual

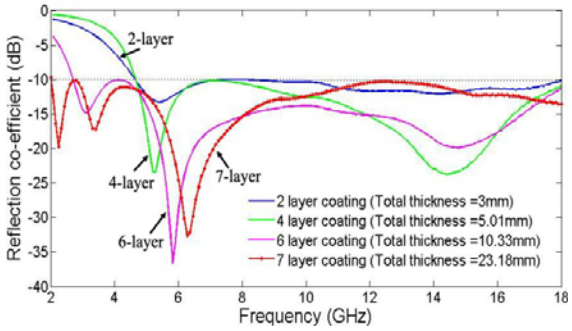

Figure 9. Reflection coefficient of multilayer absorber backed by a PEC plate for different number of layers.

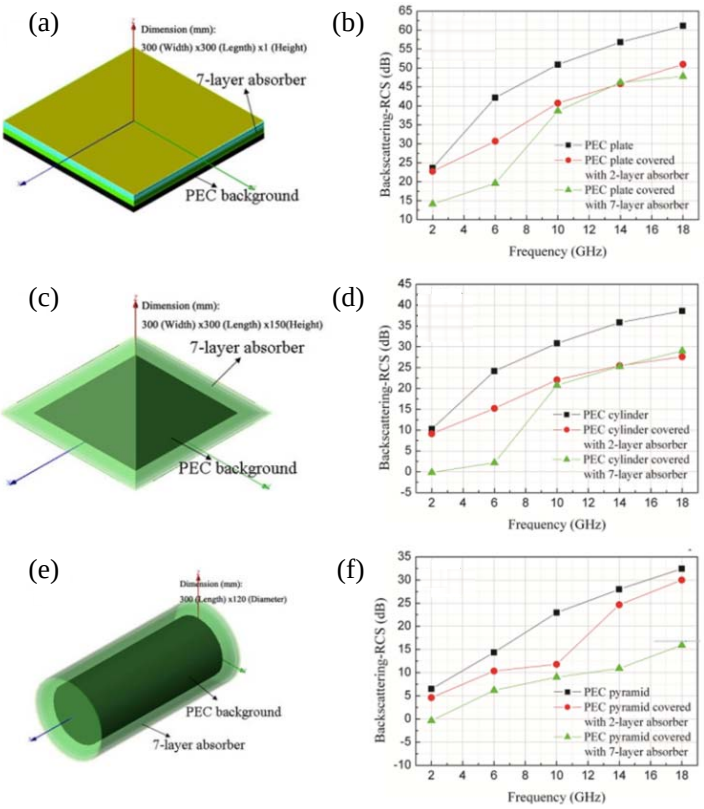

Figure 10. Back-scattering RCS of PEC objects: (a), (b) plate, (c), (d) pyramid, and (e), (f) cylinder covered with 2 and 7-layer absorbers.

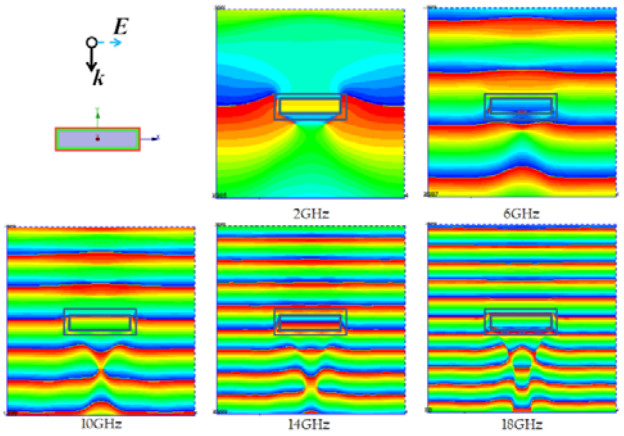

Figure 11. Phase behavior of the E-field near the rectangular PEC cylinder, which is wrapped around by an absorber blanket, normally incident on the cylinder.

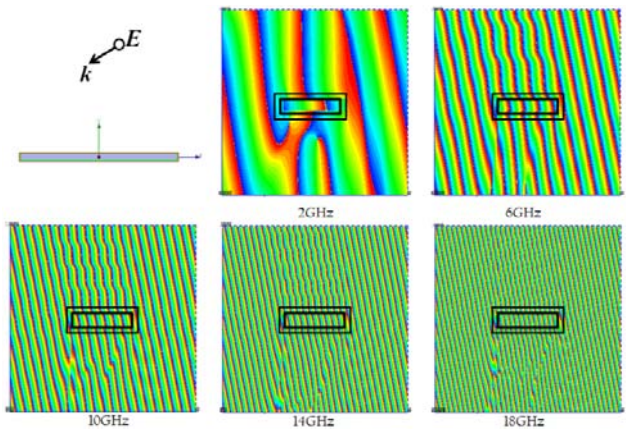

Figure 12. Phase behaviors of the E-field near the rectangular PEC cylinder, which is wrapped around by an absorber blanket, for an obliquely incident plane wave.

domain, surrounding the object, is no longer free-space, as was the case shown in Figure 5. Note also that the dimensions of the objects in the two domains are comparable, and are totally different from the legacy TO-design case, in which the scale factor between the dimensions of the object in the physical and virtual domains tends to infinity to render the target invisible.

To find the parameters of the cloak for the modified geometry in Figure 14, we revisit the integral

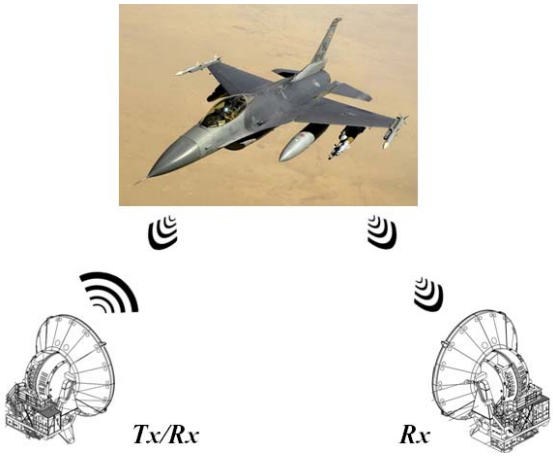

Figure 13. Target detection in conventional radar scenarios: mono-static and bi-static scheme.

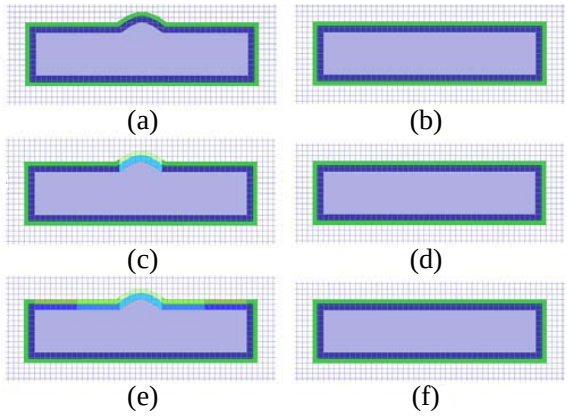

Figure 14. (a), (b) Original 2-layer absorber wrapped around a rectangular cylinder with (a) shape perturbation; (c), (d) 2-layer absorber with TO-modified material properties around regions with (c) the shape perturbation; (e), (f) 2-layer absorber with TO modified material properties for (e) all regions and 2-layer absorber wrapped around (f) a rectangular cylinder.

forms of Maxwell's Equations, presented earlier in (2a) and (2b), to relate the material parameters associated with the two systems shown in the figure. Figures 14(a), (c), (e) show the physical system with locally modified medium parameters for the perturbed object, while Figures 14(b), (d), (f) depict the virtual system with the original medium parameters covering the unperturbed object. The field distribution near the perturbed object would obviously be different from that of its unperturbed counterpart, since the perturbation introduces additional scattering to the incoming wave. We link the change in the field with the modification in the geometry, and then compensate it by the changing the medium parameters, which are illustrated by a slight change of colors from the ones representing the original planar design in Figure 14(a). Given the specific profile of the perturbation and the simulated field distributions, the only unknowns, namely the medium parameters, can be derived as follows:

$$\mu_1 = \frac{\oint E_1 \cdot dl_1}{-\frac{\partial}{\partial t}\iint H_1 \cdot dS_1} = \frac{\oint E_2 \cdot dl_1}{-\frac{\partial}{\partial t}\iint H_2 \cdot dS_1} = \frac{\oint E_2 \cdot dl_1}{-\frac{\partial}{\partial t}\iint H_2 \cdot dS_1} \cdot \left(\frac{-\frac{\partial}{\partial t}\iint H_2 \cdot dS_2}{\oint E_2 \cdot dl_2} \cdot \frac{\oint E_2 \cdot dl_2}{-\frac{\partial}{\partial t}\iint H_2 \cdot dS_2} \right)$$
$$\mu_1 = \frac{\oint E_2 \cdot dl_1}{\oint E_2 \cdot dl_2} \cdot \frac{-\frac{\partial}{\partial t}\iint H_2 \cdot dS_2}{-\frac{\partial}{\partial t}\iint H_2 \cdot dS_1} \cdot \mu_2 \tag{5a}$$

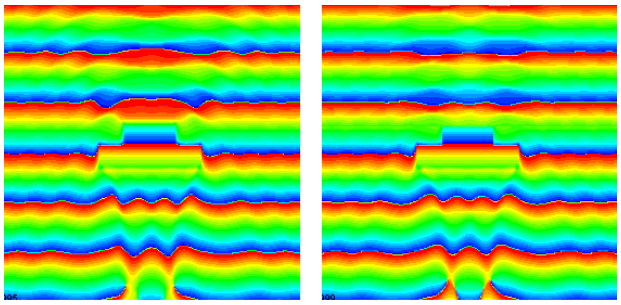

(a) (b)

Figure 15. Phase behavior of scattered E-field for (a) perturbed object wrapped by blanket with original medium parameter; (b) perturbed object wrapped by blanket with locally modified medium parameter.

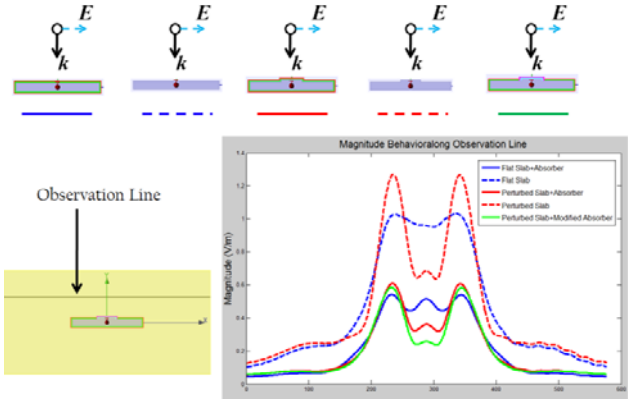

Figure 16. Comparison of the amplitudes of electric fields scattered by different objects.

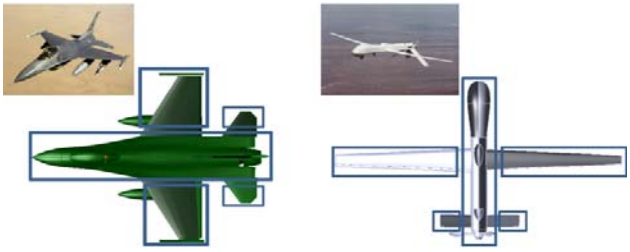

(a) (b)

Figure 17. Possible domain decomposition of two aircrafts: (a) F-16 Falcon fighter jet and (b) Predator Drone UAV for scattering-reduction treatment.

and

$$\epsilon_1 = \frac{\oint H_2 \cdot dl_1}{\oint H_2 \cdot dl_2} \cdot \frac{+\frac{\partial}{\partial t} \iint E_2 \cdot dS_2}{+\frac{\partial}{\partial t} \iint E_2 \cdot dS_1} \cdot \epsilon_2 \tag{5b}$$

where, for simplicity, we have used scalar quantities in (5) as though the geometry under consideration is two-dimensional, which it is in the present example, and we would need to replace the field quantities with vectors and the material parameters with tensors for the general 3D case.

The field behaviors for the perturbed object with locally modified material parameters can be seen from Figures 15 and 16. Figure 15 shows that the amplitude of the scattered E-field is reduced, and that the phase front of the total E-field is approximately restored as well in the reflection region. Figure 16 compares the amplitudes of the scattered electric fields for five different scenarios listed in the figure.

We should clarify the fact that although we are referring to this geometry as a slab, what we are really dealing with is a wide rectangular cylinder, with a small thickness.

We note that the modified slab does introduce additional scattering, and that the absorber does help reduce the same. We also note that the modified absorber improves the performance over the initial one, but only slightly, which shows that the planar version of the cloak is not all that inferior to the one modified for this type of geometry. Additional optimization of the modified cloak is expected to improve the performance even further, if so desired.

For an arbitrary target, we can first decompose the geometry of the target in a manner illustrated in Figure 17 into several large "blocks" that closely resemble previously investigated objects, and wrap each part of the target with an absorber, designed by using the approach based on shape perturbation

of a related smooth object. We then follow the methodology we have described above to determine the material parameters of the coating. It should be evident that this is a far more realistic approach than transforming the geometries of these complex objects into an infinitesimally small-size target, as called for by the TO algorithm for cloak designs, and following the TO recipe corresponding to such a geometry transformation, which is bound to lead to unrealistic and impractical material parameters and/or structural elements.

Modifying the permittivity and permeability parameters of the lossy materials is not the only approach one could take to reducing the scattering from objects that have curved profiles, especially when laboratory resources to fine-tune the material parameters in accordance with (5a) and (5b) are not available.

Changing the composition of the absorber can be quite effective for enhancing the absorbing performance of the coating. Figure 18 shows the RCS results of a PEC cylinder of radius 3 cm, illuminated by a plane wave. The bi-static RCS evaluated at 10 GHz, which corresponds to a wavelength of 3 cm. Various thickness compositions are analyzed to determine the one most suited for this particular cylinder, while the total thickness of the absorber is kept unchanged at 3 mm.

Figure 19 shows the result for another example of a PEC sphere of radius 30 cm illuminated by a plane wave. The bi-static RCS is again calculated at 10 GHz. Various thickness compositions are analyzed to determine the one that provides an optimal performance. Once again, the total thickness

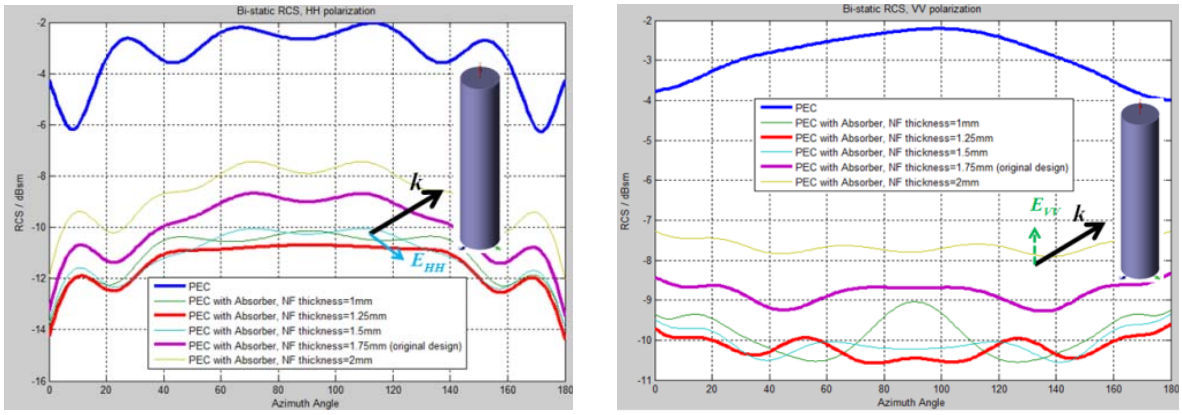

(a) (b)

Figure 18. Comparison of bi-static RCS for a long PEC cylinder coated with absorbers with various thickness compositions, for (a) horizontally and (b) vertically polarized illumination.

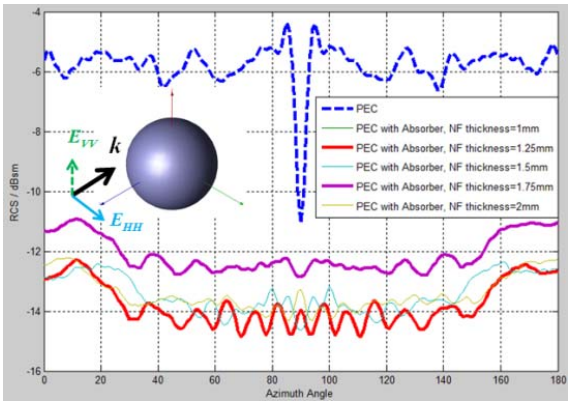

Figure 19. Comparison of bi-static RCS for a PEC sphere coated with absorber with various thickness compositions.

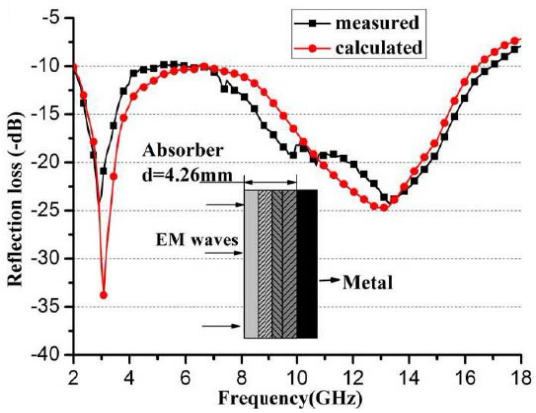

Figure 20. Calculated and measured reflection coefficient of a five-layer absorber.

of the absorber is kept unchanged at 3 mm.

We note from the figures that the optimal choice for a planar absorber is not necessarily the best one for a curved object. A moderate performance enhancement in terms of absorption can be achieved by simply changing the thickness of the absorber, as we might expect.

It should be pointed out that layered absorbing materials, which comprise of more than two types of lossy components, and/or more than two layers, are likely to be better suited for the task of coating objects with a curved profile. Figure 20 shows the example of a five-layer absorber designed for a planar surface using the optimization techniques discussed previously. Wideband absorption performance is achieved from 2 to 16.9 GHz with a total thickness of 4.26 mm (as opposed to a frequency range of 4.6 to 18 GHz and a total thickness of 3 mm) [39]. The increased number of layers provides increased degrees of freedom, which could potentially achieve the required level of performance without having to resort to synthesis of new material.

Optimization techniques can still be efficiently applied to design absorptive coatings for objects with cylindrical or spherical shapes, since the fields scattered from these canonical shapes can be analytically expressed as functions of the material parameters and compositions of the coatings. When the shapes of the objects are no longer canonical, as in the case in real-world scenarios, applying optimization technique may be a time-consuming task. This is because the forward problem, namely solving for the electric field distribution through numerical simulation — since analytical calculation is not an option

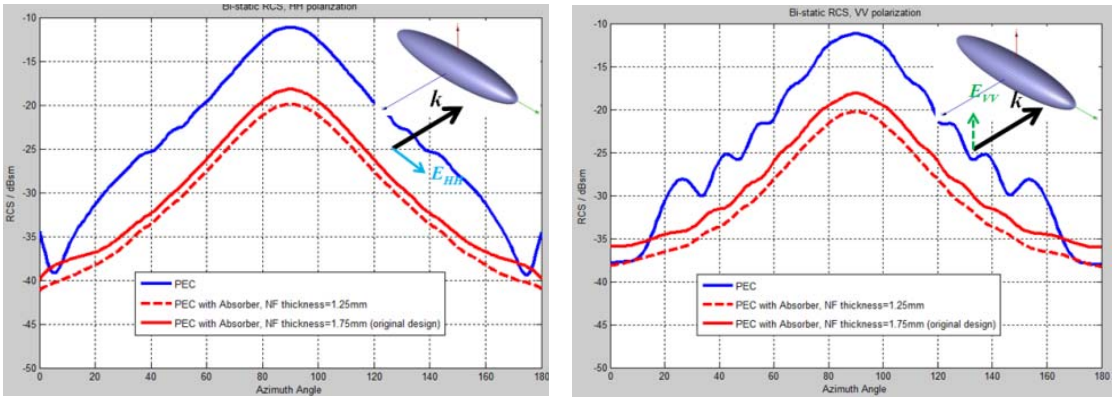

Figure 21. Comparison of bi-static RCS for a PEC ellipsoid coated with absorber of various thickness compositions, under (a) horizontally and (b) vertically polarized illumination.

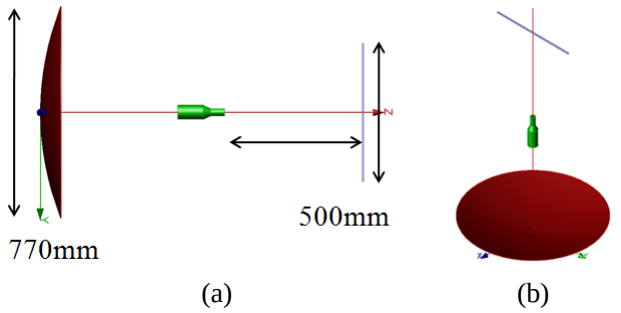

Figure 22. Model schematics for the blockage problem: (a) side view and (b) isometric view of the victim antenna (parabolic dish) and the aggressor antenna (monopole) sharing the same platform.

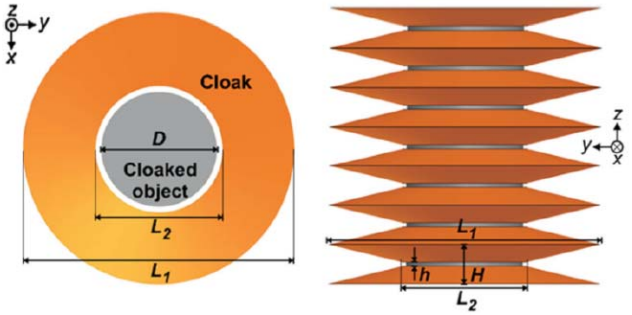

Figure 23. Model schematics for the alternative cloak.

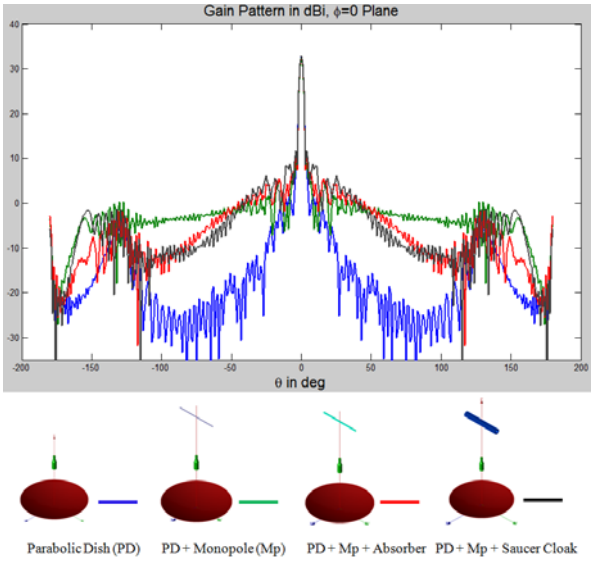

Figure 24. Radiation patterns for the antenna blockage problem: (blue) dish antenna, (green) dish antenna and the monopole antenna in the vicinity and (red) dish antenna with absorber-treated monopole antenna.

here — needs to be carried out for each and every object, for which we are designing the absorber. It is typically computer-intensive, and costly both in terms of CPU time and memory. Thus the use of powerful optimization algorithms is highly recommended for designing these absorbers.

Figure 21 shows the results for a PEC ellipsoid whose major and minor axes are 15 cm, 3 cm and 3 cm respectively and which is illuminated by a plane wave with horizontal and vertical polarizations. The bi-static RCS is calculated at 10 GHz, which corresponds to a wavelength of 3 cm. Two absorber compositions are analyzed to investigate the performances of these two configurations. The first one of these uses the original absorber design for the planar structure, while the second corresponds to the optimal thickness composition we presented in Figures 18 and 19. The total thicknesses of the two configurations are kept unchanged at the value of 3 mm in both cases.

It is evident from Figure 21 that the modified composition exhibits a slightly enhanced performance for both polarizations. However, we should point out that there is no guarantee that an improvement can always be achieved over that of the original planar design, and that an optimal design for the absorber coating can indeed be derived for a given object by simply varying the layer thicknesses using a trial-and-error approach. An alternative technique is to modify the material parameters, as illustrated above, which provides a more straightforward solution, especially for geometries shaped like the ellipsoids.

Reduction of RFI, another important application for the absorber-wrapping strategy is to mitigate the problem of antenna blockage in a shared-platform environment, as shown in Figure 22, in which the introduction of the aggressor antenna can raise the far-end sidelobe levels of the parabolic dish significantly. To mitigate this effect, we can wrap the monopole by using a multilayer absorber optimized for a planar geometry, as we have done in the past, or we can optimize the layer thicknesses and material parameter for the circular cylinder geometry. Alternatively, we can use a conducting saucer-like structure wrapped around the monopole, as proposed in [29–31]. Figure 23 shows the model used to construct the alternative cloak with the monopole as the cloaked target. Figure 24 shows the far-field patterns of a parabolic dish antenna — the victim antenna — when a monopole, which is the aggressor antenna, is placed in the vicinity of the dish. The patterns of the dish/monopole composite are also included in the figure for two treatment plans applied to the aggressor antenna. We note that the introduction of the absorber treatment reduces the sidelobe levels of the dish antenna, as compared to the case for the far-end antenna combination without the treatment.

However, we also note that an elaborate cloak design, shown in Figure 23, isn't really needed, and same level of performance can be achieved with a thin absorber type of coating.

Recent advances in material engineering and research in graphene-based absorbing materials also broadens the choice of the materials used for the absorber designs discussed in this paper. Graphene-based absorbing materials generate sufficient level of magnetic loss without the need to introduce magnetic elements such as Co, Fe and Ni. These new materials also have the advantage of being lightweight and thin, which are highly desired attributes for airborne applications. There have been reported cases of achieving below −70 dB reflection level shielding with 2.09 mm of graphene nanoplatelet-synthesized material [32], as well as below −20 dB reflection level over the entire 4.5–18 GHz with 8 mm of multilayered carbon nanotube fabric [33].

The performance of the absorbers can also be enhanced by introducing FSS-type structures within the layers [41], which add virtually no extra thickness to the composite structure. The FSS structures can be tailored to enhance the absorption in target frequency bands [34] or to broaden the working bandwidth [33, 35] of the initial layered absorber.

4. CONCLUSIONS

In this paper, we have presented a strategy for designing cloaks and absorbing coatings for scattering reduction which deviates from the classical TO algorithm. We have discussed the limitations of the Transformation Optics-based algorithm for designing cloaks, which typically calls for metamaterials that are not available in nature and suffer from problems of narrow bandwidths, high losses, unacceptable levels of polarization and incident-angle sensitivities, etc., when synthesized artificially. We have provided an alternative approach to TO for relating the material parameters of the physical and virtual domains, by using the integral forms of Maxwell's equations. We have used this new perspective to identify the root cause of the difficulty that arises when designing cloaks by using the TO; namely the inability to realize extreme values of the material parameters called for by the TO algorithm.

Following this, we have shown how we can develop absorbing coatings for planar conducting structures, and then used it as a stepping stone for designing absorbing blankets for objects of arbitrary shape.

Finally, we have detailed an algorithm for deriving the material parameters of absorbing blankets for arbitrarily shaped objects, to reduce their scattering levels in the reflection region, over a wide frequency band, and for wave incidences with arbitrary polarization and incident angles. An alternative approach to change the thickness composition of the absorbers has also been discussed. A number of examples have been included to illustrate the performances achieved by the absorbing coatings designed by using the developed technique.

REFERENCES

1. Valentine, J., J. Li, T. Zentgraf, G. Bartal, and X. Zhang, "An optical cloak made of dielectrics," *Nature Mater.*, Vol. 8, 568, 2009.
2. Leonhardt, U. and T. Tyc, "Broadband invisibility by non-euclidean cloaking," *Science*, Vol. 323, 110–112, 2009.
3. Schurig, D., J. B. Pendry, and D. R. Smith, "Calculation of material properties and ray tracing in transformation media," *Opt. Express*, Vol. 14, 9794–9804, 2006.
4. Pendry, J. B., D. Schurig, and D. R. Smith, "Controlling electromagnetic fields," *Science*, Vol. 312, 1780–1782, 2006.
5. Chen, H., B. Wu, B. Zhang, and J. A. Kong, "Electromagnetic wave interactions with a metamaterial cloak," *Phys. Rev. Lett.*, Vol. 99, 063903, 2007.
6. Smith, D. R., Y. Urzhumov, N. B. Kundtz, and N. I. Landy, "Enhancing imaging systems using transformation optics," *Opt. Express*, Vol. 18, 21238, 2010.
7. Cummer, S. A., B. Popa, D. Schurig, D. R. Smith, and J. Pendry, "Full-wave simulations of electromagnetic cloaking structures," *Phys. Rev. E*, Vol. 74, 036621, 2006.
8. Li, J. and J. B. Pendry, "Hiding under the carpet: A new strategy for cloaking," *Phys. Rev. Lett.*, Vol. 101, 203901, 2008.

9. Schurig, D., J. J. Mock, B. J. Justice, S. A. Cummer, J. B. Pendry, A. F. Starr, and D. R. Smith, "Metamaterial electromagnetic cloak at microwave frequencies," *Science*, Vol. 314, 977–980, 2006.
10. Leonhardt, U., "Optical conformal mapping," *Science*, Vol. 312, 1777–1780, 2006.
11. Kwon, D.-H. and D. H. Werner, "Transformation electromagnetics: An overview of the theory and applications," *IEEE Antennas and Propagation Magazine*, Vol. 52, No. 1, 24–46, 2010.
12. Yang, R., W. Tang, and Y.Hao, "A broadband zone plate lens from transformation optics," *Opt. Express*, Vol. 19, No. 13, 12348–12355, 2011.
13. Ruan, Z. and S. Fan, "Superscattering of light from subwavelength nanostructures," *Phys. Rev. Lett.*, Vol. 105, 013901, 2010.
14. Ergin, T., N. Stenger, P. Brenner, J. B. Pendry, and M. Wegener, "Three-dimensional invisibility cloak at optical wavelengths," *Science*, Vol. 328, 337–339, 2010.
15. Chen, H. Y. and C. T. Chan, "Transformation media that rotate electromagnetic fields," *Appl. Phys. Lett.*, Vol. 90, 241105, 2007.
16. Leonhardt, U. and T. G. Philbin, "Transformation optics and the geometry of light," *Prog. Opt.*, Vol. 53, 69–152, 2009.
17. Chen, H., C. T. Chan, and P. Sheng, "Transformation optics and metamaterials," *Nature Mater.*, Vol. 9, 387–396, 2010.
18. Huidobro, P. A., M. L. Nesterov, L. Martín-Moreno, and F. J. García-Vidal, "Transformation optics for plasmonics," *Nano Lett.*, Vol. 10, 1985–1990, 2010.
19. Edwards, B., A. Alu, M. G. Silveirinha, and N. Engheta, "Experimental verification of plasmonic cloaking at microwave frequencies with metamaterials," *Phys. Rev. Lett.*, Vol. 103, 153901, 2009.
20. Alu, A. and N. Engheta, "Achieving transparency with plasmonic and metamaterial coatings," *Phys. Rev. E*, Vol. 72, 016623, 2005.
21. Luo, Y., J. Zhang, H. Chen, S. Xi, and B.-I. Wu, "Cylindrical cloak with axial permittivity/permeability spatially invariant," *Appl. Phys. Lett.*, Vol. 93, 033504, 2008.
22. Xi, S., H. Chen, B. Zhang, B.-I. Wu, and J. A. Kong, "Route to low-scattering cylindrical cloaks with finite permittivity and permeability," *Phys. Rev. B*, Vol. 79, 155122, 2010.
23. Alu, A., A. D. Yaghjian, R. A. Shore, and M. G. Silveirinha, "Causality relations in the homogenization of metamaterials," *Phys. Rev. B*, Vol. 84, 054305, 2011.
24. Cheng, Q., T. Cui, W. Jiang, and B. Cai, "An omnidirectional electromagnetic absorber made of metamaterials," *New J. Phys.*, Vol. 12, 063006, 2010.
25. Zentgraf, T., Y. Liu, M. H. Mikkelsen, J. Valentine, and X. Zhang, "Plasmonic Luneburg and Eaton lenses," *Nature Nano.*, Vol. 6, 151–155, 2011.
26. Narimanov, E. E. and A. V. Kildishev, "Optical black hole: Broadband omnidirectional light absorber," *Appl. Phys. Lett.*, Vol. 95, 041106, 2009.
27. Gong, Y. X., L. Zhen, J. T. Jiang, C. Y. Xu, and W. Z. Shao, "Synthesis and microwave electromagnetic properties of CoFe alloy nanoflakes prepared with hydrogen-thermal reduction method," *J. Appl. Phys.*, Vol. 106, 064302, 2009.
28. Zhen, L., Y. X. Gong, J. T. Jiang, C. Y. Xu, W. Z. Shao, P. Liu, and J. Tang, "Synthesis of $CoFe/Al_2O_3$ composite nanoparticles as the impedance matching layer of wideband multilayer absorber," *J. Appl. Phys.*, Vol. 109, 07A332, 2011.
29. Tretyakov, S., P. Alitalo, O. Luukkonen, and C. Simovski, "Broadband electromagnetic cloaking of long cylindrical objects," *Phys. Rev. Lett.*, Vol. 103, 103905, 2009.
30. Alitalo, P. and S. A. Tretyakov, "Electromagnetic cloaking of strongly scattering cylindrical objects by a volumetric structure composed of conical metal plates," *Phys. Rev. B*, Vol. 82, 245111, 2010.
31. Vehmas, J., P. Alitalo, and S. A. Tretyakov, "Experimental demonstration of antenna blockage reduction with a transmission-line cloak," *IET Microwaves, Antennas & Propagation*, Vol. 6, No. 7, 830–834, 2012.
32. De Bellis, G., I. M. De Rosa, A. Dinescu, M. S. Sarto, and A. Tamburrano, "Electromagnetic absorbing nanocomposites including carbon fibers, nanotubes and graphene nanoplatelets," *2010 IEEE International Symposium on Electromagnetic Compatibility (EMC)*, 202–207, 2010.

33. Tellakula, R. A., V. K. Varadan, T. C. Shami, and G. N. Mathur, "Carbon fiber and nanotube based composites with polypyrrole fabric as electromagnetic absorbers," *Smart Mater. Struct.*, Vol. 13, 1040–1044, 2004.
34. Zhou, Y. and R. Mittra, "Performance enhancement of RF absorbers by using resistively-loaded periodic screens," *2012 IEEE Antennas and Propagation Society International Symposium (APS-URSI)*, 1–2, Jul. 8–14, 2012.
35. Mittra, R. and Y. Zhou, "Designing cloaks and absorbing blankets for scattering reduction using field and impedance transformation techniques," *Computational Electromagnetics, Recent Advances and Engineering Applications*, Chapter 14, R. Mittra, Ed., Springer, 2014, ISBN 978-1-4614-4381-0.
36. Ozgun, O. and M. Kuzuoglu, "Electromagnetic metamorphosis: Reshaping scatterers via conformal anisotropic metamaterial coatings," *Microwave Opt. Technol. Lett.*, Vol. 49, 2386–2392, 2007.
37. Ozgun, O. and M. Kuzuoglu, "Utilization of anisotropic metamaterial layers in waveguide miniaturization and transitions," *IEEE Microwave and Wireless Components Letters*, Vol. 17, 754–756, 2007.
38. Teixeira, F. L., "Closed-form metamaterial blueprints for electromagnetic masking of arbitrarily shaped convex PEC objects," *IEEE Antennas Wireless Propagat. Lett.*, Vol. 6, 163–164, 2007.
39. Qing, Y., W. Zhou, S. Huang, Z. Huang, F. Luo, and D. Zhu, "Evolution of double magnetic resonance behavior and electromagnetic properties of flake carbonyl iron and multi-walled carbon nanotubes filled epoxy-silicone," *Journal of Alloys and Compounds*, Vol. 583, 471–475, 2014.
40. Haupt, R. L. and D. H. Werner, *Genetic Algorithms in Electromagnetics,* John Wiley & Sons, 2007.
41. Munk, B. A., *Frequency Selective Surfaces: Theory and Design,* Wiley, New York, 2000.
42. Argyropoulos, C., E. Kallos, Y. Zhao, and Y. Hao, "Manipulating the loss in electromagnetic cloaks for perfect wave absorption," *Opt. Express*, Vol. 17, 8467–8475, 2009.
43. Argyropoulos, C., E. Kallos, and Y. Hao, "FDTD analysis of the optical black hole," *J. Opt. Soc. Am. B*, Vol. 27, 2020–2025, 2010.
44. Kwon, D.-H., "Transformation electromagnetics and optics," *Forum for Electromagnetic Research Methods and Application Technologies (FERMAT)*, Vol. 1, 2014.